Flow Dynamics in a Supersonic Diffuser at Minimum Starting Condition to Simulate Rocket's High Altitude Test on the Ground

*Hyowon Yeom, Sangkyu Yoon, Hong-Gye Sung**
Korea Aerospace University, Goyang, Gyeonggi, 412-791, South Korea
Yongwook Kim and Seunghyup Oh
Korea Aerospace Research Institute, Taejon, 305-600, South Korea

hgsung@kau.ac.kr

Keywords: Supersonic Diffuser, High Altitude Test, Shock Train, Vacuum Pressure, Unsteady CFD

Abstract

A numerical analysis has been conducted to investigate and characterize the unsteadiness of flow structure and oscillatory vacuum pressure inside of a supersonic diffuser equipped to simulate the high-altitude rocket test on the ground. A physical model of concern includes a rocket motor, a vacuum chamber, and a diffuser, which have axisymmetric configurations, using nitrogen gas as a driving fluid. Emphasis is placed on investigating physical phenomena of very complex and oscillatory flow evolutions in the diffuser operating at very close to the starting condition, i.e. minimum starting condition, which is one of major important parameters in diffuser design points of view.

I. Introduction

A rocket motor designed for operation at high altitude needs a nozzle with a large expansion ratio to maximize thrust at much lower atmospheric pressure than that at sea level. When these motors are tested on the ground, accurate performance can't be proved due to flow separation occurring in the nozzle. Therefore, to evaluate accurate performance of such rocket motors, a high altitude test facility system is required to test a rocket motor at high altitude conditions on ground. One system is a supersonic exhaust diffuser and another is an ejector to simulate high altitude conditions on ground. The simplest method of these is using the supersonic exhaust diffuser.

The study on tests, design methods, and the internal flow of experimental systems simulating high altitude conditions has been performed in research institutes, industries and academic labs since the mid-1950s. In the US, experiments and theoretical analysis about various performance factors were performed for the research and development of ground experimental equipment simulating high altitude condition at the government sponsored AEDC (Arnold Engineering Development Center)[1,2,3]. The AEDC proposed theoretical methods for determining the starting pressure of various types of diffuser (long cylindrical diffuser, long second throat diffuser, short second throat diffuser, etc.) [1,2,3,4]. In India, for the design of a high altitude test (HAT) facility for testing the third stage motor (Ps-3) of Polar Satellite Launch Vehicle, experiments using both cold nitrogen gas and hot rocket exhaust gas as driving fluids were carried out in the ISRO (Indian Space Research Organization)[8]. In France, the DGA/CAEPE developed the high altitude test facility MESA consisting of a vacuum pump, ejector and diffuser. In order to find the optimum configuration, four diffuser experiments were performed by ONERA R1Ch facility. Numerical analysis was conducted to evaluate experimental data performed by ONERA R1Ch facility [9]. In the most recent research, Perdue University developed a lab-scale high altitude facility in order to supply a hybrid rocket motor with an air-powered ejector and blow-off door for the initial lower back pressure [10].

For this paper, numerical simulation was conducted in order to comprehend the detail flow evolution information in the diffuser operating at minimum starting condition, which blinded in experiments, but very important in diffuser design points of view. The minimum starting pressure is one of the major factors for determination of the size of test facility such as driving fluid supply system, the rocket and diffuser sizes, and so on.

II. Numerical Method

A. Governing Equation

The Farve averaged governing equations based on the conservation of mass, momentum, and energy for a compressible, chemically reacting gas can be written as

$$\frac{\partial \bar{\rho}}{\partial t} + \frac{\partial \bar{\rho}\tilde{u}_j}{\partial x_j} = 0 \tag{1}$$

$$\frac{\partial \bar{\rho}\tilde{u}_i}{\partial t} + \frac{\partial\left(\bar{\rho}\tilde{u}_i\tilde{u}_j + \bar{p}\delta_{ij}\right)}{\partial x_j} = \frac{\partial\left(\bar{\tau}_{ij} - \overline{\rho u_j'' u_i''}\right)}{\partial x_j} \tag{2}$$

$$\frac{\partial \bar{\rho}\tilde{E}}{\partial t} + \frac{\partial\left(\left(\bar{\rho}\tilde{E} + \bar{p}\right)\tilde{u}_j\right)}{\partial x_j} = \frac{\partial\left(\tilde{u}_i\bar{\tau}_{ij} - \overline{\rho h'' u_i''}\right)}{\partial x_j} - \frac{\partial \bar{q}_j}{\partial x_j} \tag{3}$$

B. Turbulence Closure

The standard k-ε model was proposed for high Reynolds number flows and is traditionally used with a wall function and the variable y^+ as a damping function. Universal wall functions do not exist in

complex flows, however, and the damping factor cannot be applied to flows with separation. Thus, a low Reynolds number k-ε model was developed for near-wall turbulence. Within certain distances from the wall, all energetic large eddies will reduce to Kolmogorov eddies (the smallest eddies in turbulence), and all the important wall parameters, such as friction velocity, viscous length scale, and mean strain rate at the wall, can be characterized by the Kolmogorov micro scale.

Yang and Shih[11] proposed a time-scale-based k-ε model for the near-wall turbulence related to the Kolmogorov time scale as its lower bound, so that the equation can be integrated to the wall. The advantages of this model are (a) no singularity at the wall, and (b) adaptability to separation flow, since the damping function is based on the Reynolds number instead of y^+. The low Reynolds number models have been designed to maintain the high *Re* formulation in the log-law region and further tuned to fit measurements for the viscous and buffer layers. The low Reynolds number model used in this work is based on Yang and Shih.

The turbulent kinetic energy and its dissipation rate are calculated from the turbulence transport equations written in the following:

$$\frac{\partial \bar{\rho}\tilde{k}}{\partial t}+\frac{\partial\left(\bar{\rho}\tilde{u}_j\tilde{k}\right)}{\partial x_j}=\frac{\partial}{\partial x_j}\left(\left(\mu+\frac{\mu_t}{\sigma_k}\right)\frac{\partial \tilde{k}}{\partial x}\right)+P_k-\bar{\rho}\tilde{\varepsilon} \quad (4)$$

$$\frac{\partial \bar{\rho}\tilde{\varepsilon}}{\partial t}+\frac{\partial\left(\bar{\rho}\tilde{u}_j\tilde{\varepsilon}\right)}{\partial x_j}=\frac{\partial}{\partial x_j}\left(\left(\mu+\frac{\mu_t}{\sigma_\varepsilon}\right)\frac{\partial \tilde{\varepsilon}}{\partial x}\right)+\frac{\left(C_{\varepsilon 1}P_k-C_{\varepsilon 2}\bar{\rho}\tilde{\varepsilon}\right)}{T_t}+\Lambda \quad (5)$$

Where, P_k, T_t and Λ are each turbulent kinetic energy production rate, turbulent time scale and damping function and then represented as follows:

$$P_k=\left(\mu_t\left(\frac{\partial \tilde{u}_i}{\partial x_j}+\frac{\partial \tilde{u}_j}{\partial x_i}-\frac{2}{3}\frac{\partial \tilde{u}_k}{\partial x_k}\delta_{ij}\right)-\frac{2}{3}\bar{\rho}\tilde{k}\delta_{ij}\right)\frac{\partial \tilde{u}_i}{\partial x_j} \quad (6)$$

$$T_t=\frac{\tilde{k}}{\tilde{\varepsilon}}+\tau_k \quad (7)$$

$$\tau_k=C_k\left(\frac{\nu}{\varepsilon}\right)^{1/2} \quad (8)$$

$$\Lambda=\nu\mu_t\left(\frac{\partial \tilde{u}_i}{\partial x_j \partial x_k}\right)^2 \quad (9)$$

where τ_k is Kolmogorov time scale.

The turbulent viscosity and damping factor f_μ for wall effect can be written as

$$\mu_t=\bar{\rho}C_\mu f_\mu \tilde{k}T_t \quad (10)$$

$$f_\mu=\left[1-exp\left(-a_1R_y-a_3R_y{}^3-a_5R_y{}^5\right)\right]^{1/2} \quad (11)$$

Damping factor is taken to be a function of $R_y=k^{1/2}y/\nu$.

Following constants are used.

$\sigma_k=1.0$, $\sigma_\varepsilon=1.3$, $C_\mu=0.09$,

$C_{\varepsilon 1}=1.44$, $C_{\varepsilon 2}=1.92$

$a_1=1.5\times10^{-4}$, $a_3=5.0\times10^{-7}$, $a_5=1.0\times10^{-10}$

C. Numerical Scheme

The conservation equations for moderate and high Mach number flows are well coupled, and standard numerical techniques perform adequately. In regions of low Mach number flows, however, the energy and momentum equations are practically decoupled and the system of conservation equations becomes stiff. In the entire diffuser system, the flow fields are governed by a wide variety of time scales (from supersonic flow of the rocket jet to stagnation-flow in the vacuum chamber). Such a wide range of time scales causes an unacceptable convergence problem. The author experienced the conventional numerical scheme could not calculate the vacuum chamber pressure in accurate. To overcome the problem, a dual time-integration procedure designed for all Mach number flows is applied, which may be constructed in two steps. First, a rescaled pressure term is used in the momentum equation to circumvent the singular behavior of pressure at low Mach numbers. Second, a dual time-stepping integration procedure is established.

The pseudo-time derivative may be chosen to optimize the convergence of the inner iterations through using an appropriate preconditioning matrix that is tuned to rescale the eigenvalues to render the same order of magnitude to maximize convergence. To unify the conserved flux variables, a pseudo-time derivative of the form $\Gamma\partial Z/\partial\tau$ can be added to the conservation equation. Since the pseudo-time derivative term disappears as converged, a certain amount of liberty exists in choosing the variable *Z*. We take advantage of this by introducing a pressure p' as the pseudo-time derivative term in the continuity equation:

While dual time stepping and LU-SGS are applied for time integration, control volume method is used to integrate both inviscid fluxes represented by AUSMPW+ and MUSCL and viscous fluxes by central difference. The code is paralleled with multi-block feature using MPI library to speed up the unsteady calculation.

III. Results and Discussion

A. Diffuser Configurations

Test model with a large vacuum chamber is illustrated in Fig. 1. The physical sizes of the test models were determined to investigate the effect of major design parameters, such as the area ratio of diffuser to rocket nozzle throat(A_d/A_t), the expansion ratio of rocket nozzle(A_e/A_t), and rocket

nozzle throat diameter, to start the diffuser. Experiments using cold nitrogen gas ($\gamma = 1.4$) as a driving fluid were carried out. Figure 2 shows the computational domain concerned in this study. The computational configuration is exact same as that of the experiment except the vacuum chamber configuration, but with same volume size not to lose any accuracy and promote numerical convergence rate. The computation domain consists of 3 blocks and each block grid is 115* 50, 79*30, 206*79 respectively. The wall conditions on the front of vacuum chamber, and stagnation pressure and temperature in the rocket chamber are applied respectively. The wall is assumed as adiabatic wall while partially subsonic and supersonic conditions depending on the flow condition are applied for the exit of a diffuser. Total 8 processors are participated for parallel computation.

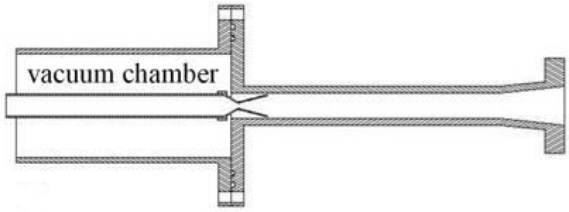

Figure 1. Schematics of a model diffuser.

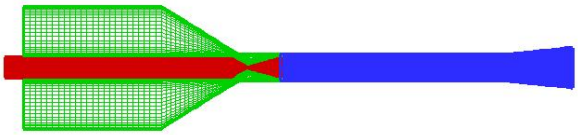

Figure 2. Computational domain consisting 3 blocks.

B. Diffuser Operations

The starting process of the supersonic exhaust diffuser can be explained through Fig. 3 in Ref. [3]. In region (1), both nozzle and diffuser are unstarted. The jet momentum exhausted from rocket is not enough for the flow to fulfill the nozzle so the flow is separats from the nozzle wall. As the P_0 / P_a increases further, the nozzle flows full but over-expands, however, so the diffuser is still unstarted in region (2). The unstarted regime consists of two phases. In the first phase, the flow separates from the nozzle wall through oblique shock, and in the second phase, the flow separation occurs at the nozzle exit. As the P_0 / P_a is further increased to the $(P_0 / P_a)_{st,min.}$, the diffuser also flows full so that the shock system is fully established in the duct. In this regime, the under expanded supersonic jet from the nozzle impinges on the diffuser wall. At this stage, the supersonic exhaust diffuser is said to have started and the corresponding pressure ratio is the minimum starting pressure ratio, $(P_0 / P_a)_{st,min.}$.

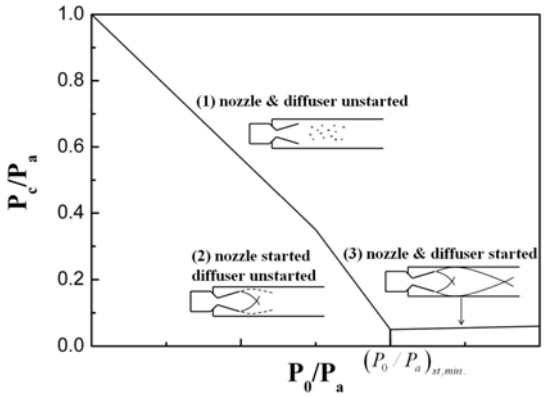

Figure 3.Typical diffuser characteristic curve Ref. [3].

In this study, above all three operation regime are simulated in case of the area ratio of diffuser cross section to nozzle throat, $A_d / A_t = 56.25\ mm$, in order to observe flow structure and validate the numerical results. At 10 bar of rocket chamber, the diffuser operation regime belongs to region (1) in Fig. 3. The flow separates inside of nozzle so that the exhaust jet can not impinge on the diffuser wall as shown in Fig. 4(a). Because the flow in the diffuser belongs to the subsonic regime, pressure along the wall increases gradually to atmospheric pressure from the somewhat low pressure at vacuum chamber due to the suction of the inside flow of vacuum chamber into the jet boundary, as shown in Fig. 3(b). Experimental values are marked as symbols and numerical values are represented as lines. Both values are in fairly good agreement. Since the mass flux of the jet at 10 bar is not enough to stat the diffuser, the rocket chamber pressure increases to 44 bar, around the starting pressure of the diffuser, then the jet exhausting from rocket nozzle impinges on the diffuser wall shown in Fig. 3(a). The pressure in vacuum chamber is evacuated to around 50 torr from 1 bar, proving that the diffuser is working. The pressure rises behind the impinging point of jet on the diffuser wall, and decreases in the expansion region and increases again next compression wave, and then finally rises to atmospheric pressure at the exit of the diffuser. The experimental data and the numerical results look like some discrepancy but the unsteady flow motions are blinked on background of the instantaneous data, which described in the next section in detail. If the motor pressure increases further, the jet strength impinging on the diffuser wall also increases as expected. The motor pressure of 50bar provides two peaks of pressure along the diffuser due to two impingements on the diffuser wall. The numerical results are fairly good comparable with the experimental data, in different view as shown at 44 bar of rocket motor. From the insight on the detail comparison, the more careful treatment on both numerical and experimental task might be necessary to avoid misleading to incomplete conclusion due to simple comparisons.

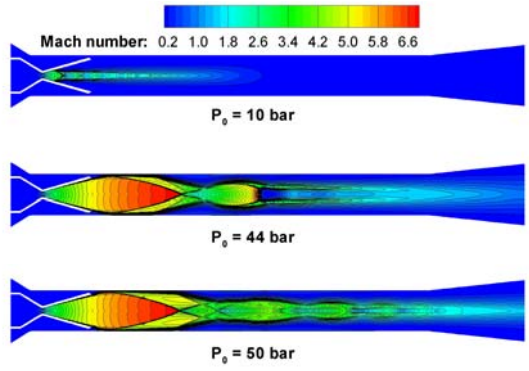

(a) Mach number contours

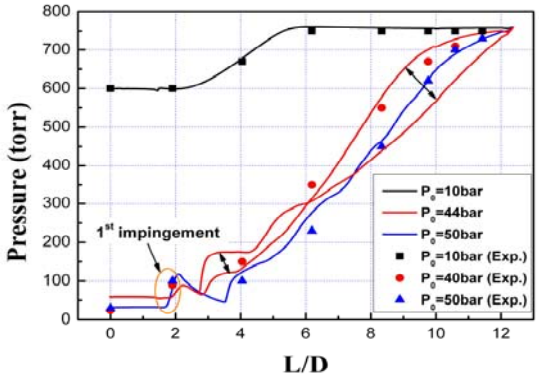

(b) Pressure distribution

Figure 4. Mach number contours and pressure distribution along the diffuser wall with $A_d / A_t = 56.25$.

C. Unsteadiness of flow structures

As described in section B, the flow structures in diffuser are classified according to three operation regimes of diffuser in global view points. In this study, detail flow structures at diffuser starting point are accurately examined because of two reasons: 1) a minimum starting pressure is the very important design parameter of a diffuser because the starting pressure affects the size of test facilities. 2) a steady calculation to investigate flow structure and to predict pressure value in diffuser may mislead to wrong decision because the exact experiments to determine a minimum starting pressure of diffuser is very critical. Figure 5 shows the flow evolution of Mach number and shadow graph at 40 bar. The normal shock moves forth and back from a reference position with 0.8 msec periodic time. The acoustic waves traveling inside of the diffuser may induce the shock train. If the rocket pressure increases to 44 bar, the shock train structure shows different figure (Fig. 6). A small supersonic pocket behind the first diamond shock is occurred at the axis of the diffuser and it moves down stream and upstream in periodic. The period of oscillation may relate with the acoustic mode in subsonic region after the first diamond shock. The length of shock is further away from the reference position than that of 40 bar. The following physical phenomena may explain the reason: 1) the mass flux at 44 bar is enough to produce the second shock pocket but not so strong as the first diamond shock. 2) the coupling of acoustic waves and flow evolution can easily excite the movement of the second shock pocket.

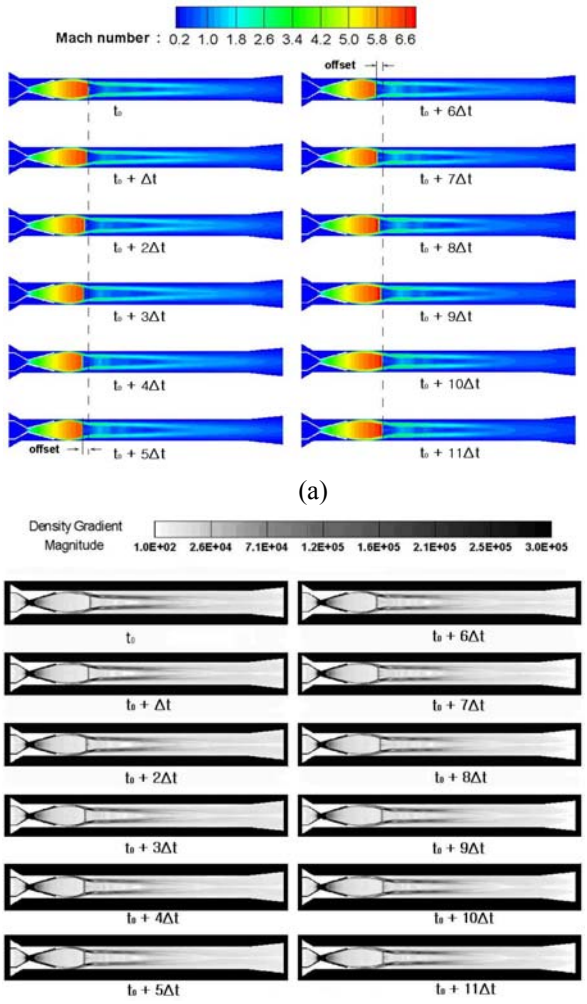

Figure 5. Flow evolution in a diffuser at motor pressure 40bar with $A_d / A_t = 56.25$ (Δt=0.1 msec): (a) Mach number contours, (b) shadowgraph.

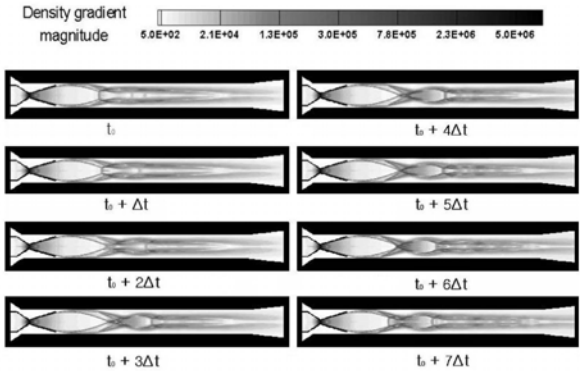

Figure 6. Flow evolution in a diffuser at motor pressure 44bar with $A_d / A_t = 56.25$ (Δt=0.1 msec).

Even though the rocket pressure keeps constant as 40 bar or 44 bar, the flow structure shows different features as described above. While only one shock pocket is generated at 40 bar, two shock pockets are for 44 bar. Since only one shock occurs at 40 bar, the pressure traveling from downstream to upstream penetrates into the vacuum chamber and provides some pressure fluctuations in the vacuum chamber as shown in Fig. 7(a). However, at 44 bar, the pressure wave traveling from downstream to upstream can not penetrate the first shock pocket so that the pressure change at the vacuum chamber is negligible as shown in Fig. 7(a): one lines of 44 bar splits to two lines after the first impingement position of the shock at different time frame. But the pressure still a little fluctuates because the pressure information can transfer into the vacuum chamber through a boundary layer, even though its strength is greatly attenuated. Figure 8 shows the shadowgraphs zoomed near the shock impingement at two pressures. At 40 bar the boundary length of the impingement and supersonic area are much shorter than those of 44 bar, which proves the above claim. Fig. 7(b) shows the pressure along the axis. The first normal shock position at 40 bar is further upstream, but the amplitude of fluctuation provides much higher value at 44 bar. It notes that the coupling between acoustic wave and flow evolution may produce over-pressurization inducing over-oscillation of test facility structure if those frequencies are exactly matched.

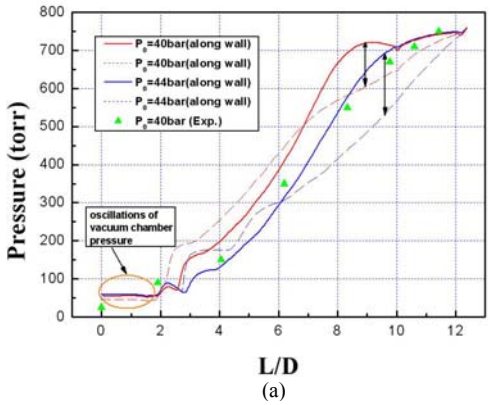

Figure 7. Pressure distribution in the diffuser both along the wall and at centerline at motor pressure 40bar and 44 bar with $A_d / A_t = 56.25$.

Figure 8. Shadowgraphs near shock impingement on the diffuser at motor pressure (a) 40bar and (b) 44 bar with $A_d / A_t = 56.25$.

VI. Conclusion

The unsteadiness of flow structure and pressure inside a supersonic diffuser to simulate rocket's high altitude test on the ground was numerically investigated by treating the conservation equations of mass, momentum, and energy. The model takes into account a compressible low-Reynolds-number κ-ε turbulent model. The computational geometry consists of the entire diffuser flow path from the rocket chamber and vacuum chamber in stagnation conditions to the exhaust of the diffuser. While dual time stepping and LU-SGS are applied for time integration, control volume method is used to integrate inviscid fluxes represented by AUSMPW+ and MUSCL and viscous fluxes by central difference. Total 8 processors are participated for parallel computation using MPI library.

Unsteady numerical calculations are quite comparable to experimental data and convey valuable information to investigate unsteadiness of diffuser operation, especially at rocket chamber pressure close to the minimum starting condition of diffuser. At 10bar, the unstart condition and 50 bar, much higher pressure than the starting pressure, the pressures along the diffuser wall show relatively steady data. If the diffuser starts, the vacuum chamber pressure has a typical value about 50 torr, which belongs to the atmospheric pressure of around 20-25 km altitude. The vacuum pressure keeps constant even though the higher rocket chamber pressure than the starting one is supplied. At minimum starting pressure, 40 bar, both the vacuum chamber pressure and the wall pressure periodically oscillates due to the shock train. However, at 44 bar, somewhat above the starting pressure, the pressure along center line shows much greater amplitudes than that in case of 40 bar, but the vacuum chamber pressure negligibly oscillates due to much larger size of the boundary length of the shock impingement and supersonic area which attenuates pressure oscillation transferring through boundary layer. This information may very valuable to determine the minimum operating pressure of the diffuser in economic and stable diffuser-design points of view.

Acknowledgement

The authors would like to thank KARI for the partial funding through the research consortium of Korea Space Launch Vechicle and TERA TEC for the supports of TERA CLUSTER resources.

References

1) Sivo, J.N., Meyer, C.L. and Peters, D.J., "Experimental Evaluation of Rocket Exhaust Diffusers for Altitude Simulation," NASA-TN-D-298, 1960.
2) Goethert, B.H., "High Altitude and Space Simulation Testing," ARS Journal, 1962, pp872-882.
3) Massier, P.F. and Roschke, E.J., "Experimental Investigation of Exhaust Diffusers for Rocket Engines," JPL-TR-32-210, 1962.
4) German, R.C., Bauer, R.C. and Panesci, J.H., "Methods for Determining the Performance of Ejector-Diffuser Systems," *Journal of Spacecraft and Rockets*, Vol. 3, No. 2, 1966, pp. 193-200.
5) Wojciechowski, C.J. and Anderson, P.G., "Parametric Analysis of Diffuser Requirements for High Expansion Ratio Space Engine," LMSC-HREC-TR-D784489, NASA-CR-161924, 1981.
6) McAmis, R. and Bartlett, C., "Aerodynamic Free-Jet Nozzle Performance Augmentation Using An Exhaust Diffuser," AIAA Paper 91-2270, 27th AIAA/ASME/SAE/ASEE Joint Propulsion Conference & Exhibit, Sacramento, CA, 1991.
7) Stephens, S.E., "Experimental and Computational Data from a Small Rocket Exhaust Diffuser," AIAA Paper 93-1860, 29th AIAA/ASME/SAE/ASEE Joint Propulsion Conference & Exhibit, Monterey, CA, 1993.
8) Annamalai, K., Visvanathan, K., Sriramulu, V., Bhaskaran, K.A., "Evaluation of the performance of supersonic exhaust diffuser using scaled down models," Experimental Thermal and Fluid Science, Vol. 17, Issue 3, July, 1998, pp.217-229.
9) Quebert, L. and Garcia, Y., "Theoretical and Experimental Design of an Exhaust Diffuser for an Upper Stage Engine of a Ballistic Missle," AIAA Paper 2001-3382, 37th AIAA/ASME/SAE/ASEE Joint Propulsion Conference & Exhibit, Salt Lake City, Utah, 2001.
10) Otterstatter, M.R., Meyer, S.E., Heister, S.D., Dambach, E.M., "Design of an Altitude-testing Facility for Lab-Scale Propulsion Devices," AIAA Paper 2007-5323, 43rd AIAA/ASME/SAE/ASEE Joint Propulsion Conference & Exhibit, Cincinnati, OH, 2007.
11) Yang, Z. and Shih, T. H., "New Time Scale Based $k-\varepsilon$ Model for Near-Wall Turbulence," *AIAA Journal*, Vol. 31, No. 7, 1993, pp. 1191- 1197.